Engineering of struvite crystals by regulating supersaturation – Correlation with phosphorus recovery, crystal morphology and process efficiency

Sina Shaddel[a],[*], Seniz Ucar[b], Jens-Petter Andreassen[b], Stein W. Østerhus[a]

[a] *Department of Civil and Environmental Engineering, Norwegian University of Science and Technology (NTNU) Trondheim, Norway*
[b] *Department of Chemical Engineering, Norwegian University of Science and Technology (NTNU) Trondheim, Norway*

ABSTRACT

Struvite crystallization is widely applied for nutrient recovery from wastewater streams. The better understanding of the effects of reaction conditions on final crystal properties will contribute to improve both the recovery efficiency and product quality of struvite as a fertilizer. In this study, batch crystallization experiments were performed in laboratory scale to reveal the effect of supersaturation on the phosphorus recovery and crystal properties. For this purpose, supersaturation is regulated through varying the pH, magnesium and ammonium concentrations in solution. The effects of these parameters on controlling crystal properties such as size and morphology are highlighted through their role as supersaturation regulators.

The potential implications of different crystal morphologies on settling velocity and aggregation of crystals are also discussed. This improved understanding could aid in improved struvite crystallization processes for wastewater treatment.

1. Introduction

Phosphorus (P) is one of the essential elements in living organisms and an irreplaceable ingredient for agricultural fertilizers that are used in crop and livestock production. However, phosphate rocks, which are the main source of P, are non-renewable and in danger of depletion [1]. In addition, beside diminishing phosphate rocks, P content has increased notably in the hydrosphere because of human activity through domestic and industrial waste, which can cause eutrophication [2]. Therefore, its efficient use, recovery and recycling are important steps towards environmental safety and a sustainable development.

P-recovery from wastewater is an effective strategy to address both problems and has gained great attention [1]. The most commonly used approach has been the precipitation of P-bearing minerals from wastewater, such as struvite (magnesium ammonium phosphate hexahydrate, $MgNH_4PO_4 \cdot 6H_2O$). Struvite has the advantages of being composed of primary macronutrient (nitrogen and phosphorus) and secondary macronutrient (magnesium), and being a slow-release fertilizer that can be used directly as precipitated [3,4]. In addition, controlled precipitation of struvite in wastewater treatment plants aids in avoiding pipe clogging and extra costs of equipment cleaning [5,6].

Efficiency of a P-recovery process and struvite product quality can be enhanced by controlling the precipitation reaction to optimize the reaction time as well as the size and morphology of the crystals. The shape and size of crystals have strong impact on the properties of final product as well as the efficiency of downstream processes like settleability, filtering and drying. Therefore, it is important to be able to tailor process conditions for optimization of these properties. It could be misleading to measure the process efficiency in terms of soluble-P removal as the fine particles can be washed-out and redissolve in downstream processes, which affect the reliability of modeling and economic predictions for the whole process [7]. Therefore, improving the efficiency of downstream processes via regulating reaction parameters enhances the phosphorus recovery efficiency and ensures the quality of effluent. The consistency in the quality and properties of final product is one of the determinative factors for the success of struvite production. The particular processes in wastewater treatment plants, feed and seasonal variations often create changes in the composition of the input material to the crystallizer. Therefore, the operational conditions should be properly adjusted to minimize the risk of fail to meet the product quality and process requirements.

Supersaturation is the main parameter that governs size and morphology of the precipitated struvite and the phosphorus recovery efficiency [8,9]. Crystal size is determined dominantly by supersaturation since the nucleation and growth kinetics are correlated with the thermodynamic driving force in the crystallizing system. The application of the kinetic models for nucleation and growth can be used to control the size related settling characteristics of struvite crystals [10]. The crystal

morphology is an outcome of the internal (crystal lattice structure and crystal defects) and external factors (supersaturation, the presence of impurities, temperature, etc.). The modification of crystal morphology has been receiving growing attention due to both theoretical interest and industrial needs [11,12]. However, a systematic correlation of struvite morphology with supersaturation and transition boundary between different morphologies for wastewater application is not yet fully explored in the literature. The dependency of struvite morphology on supersaturation, mixing energy and retention time has already been mentioned by previous studies [8,13,14]. Although it is well established that crystal morphology is highly effective on the settling velocity, this aspect has not been reported for struvite previously.

Previous work also implicitly reported the dominant effect of supersaturation on precipitation kinetics and aggregative properties of crystals [15,16]. The liquid from dewatering of anaerobically digested sludge is the main feed for the majority of struvite reactors [17]. Although, the reported studies are not directly applicable for wastewater applications due to distinct compositions and characteristics related to wastewater. The equimolar and low concentration of struvite constituents ions or the high phosphate concentrations in swine wastewater are not representative for wastewater applications.

High initial supersaturation in the vicinity of inlet ports of struvite reactor can favor nucleation over crystal growth at the onset of crystallization. Improving aggregation of the generated crystals in this stage is important; otherwise distribution of them in the space and time will reduce the chance of collision and aggregation in later stages. Moreover, improved aggregation contributes to better granulation and will further reduce the chance of product loss from reactor by wash out. While the struvite aggregation is mainly explained based on zeta potential in previous studies [18,19], the effect of initial supersaturation on crystal aggregation is mainly disregarded.

Numerous studies have investigated the feasibility of P-recovery via struvite precipitation from laboratory to pilot scale and the existing full-scale struvite crystallization techniques all advertise high recovery efficiency (80–90%) [7,19–21]. However, the impacts of operational conditions on the different characteristics of obtained products remain unclear. Thus, large-scale processes are yet to be optimized in terms of product quality and efficiency, where variations can be expected due to individual processes employed at different plants. The individual optimization of reaction parameters such as pH and struvite constituent ions (Mg^{2+}, NH_4^+) is the most common approach to enhance the phosphorus recovery. However, this approach without a clear understanding of benefits and disadvantages on product properties will not improve the overall efficiency of the process. Further, owing to the complexity of crystallization processes, considering a comprehensive parameter is necessary to consistently achieve the desired recovery efficiency and product properties. Supersaturation is an inclusive parameter independent of reactor type which takes into account the effect of several parameters (struvite constituent ions, ionic strength, pH and temperature). Although supersaturation regulation is crucial to improve the overall process performance, lack of a fundamental understanding on lumped recovery efficiency and struvite properties hindered the utilization of supersaturation as a design parameter. Therefore, coupling the recovery efficiency and product properties requires a better understanding of the role of supersaturation from a fundamental viewpoint.

The aim of this study is to explore the central role of supersaturation on phosphorus recovery efficiency and shaping product properties. Revealing the correlation between supersaturation and the size and morphology of the final precipitation products, and further evaluate their consequent effects on downstream processes is the main focus of this work.

One of the objectives of this study was to utilize the supersaturation as an inclusive parameter to couple the recovery efficiency and product properties. Therefore, the effects of impurities were eliminated by conducting the experiments with synthetic reject water that enables accurate calculation of supersaturation. Both reaction conditions and crystal properties are evaluated for discussing the final crystal morphology where supersaturation was followed as the main parameter.

In order to define a proper operational strategy for supersaturation regulation, a systematic approach was employed to investigate the effects of pH and molar ratios of constituent ions on the P-removal efficiency and product quality. By scanning through a relevant range of supersaturation values, efficient control on crystal size and morphology was attained and further correlation of these properties with settling and aggregation characteristics were evaluated. This fundamental understanding is crucial for improving full-scale applications of phosphorus recovery by struvite crystallization via optimization of operational conditions and their effects on crystal properties.

2. Materials and methods

2.1. Materials

Magnesium chloride hexahydrate ($MgCl_2 \cdot 6H_2O$), sodium dihydrogen phosphate ($NaH_2PO_4 \cdot 2H_2O$), ammonium chloride (NH_4Cl) and sodium hydroxide (NaOH) were used for the synthesis of struvite. All chemical reagents were purchased from Merck with analytical grade. Milli-Q water (18.2 MΩ.cm) was used for all purposes.

2.2. Methods

All experiments were carried out using a lab-scale crystallization system, composed of a 1 L glass reactor, stirred with Teflon two-blade propeller controlled by a mechanical stirrer operated at 200 rpm. Temperature was regulated by a water bath and maintained at $20 \pm 0.5^{\circ}$ C for all experiments. The pH was constantly measured and recorded by a combined glass electrode with KCl reference electrolyte connected to EasyDirect™ pH Software (Metrohm), and calibrations were carried out daily. The precipitation reaction was initiated by addition of $MgCl_2$ solution to a synthetic reject solution and the reactions were let to proceed for 60 min. The pH was kept constant during experiments by addition of 1 M NaOH. In the case of terminating crystallization reactions for further studies, the pH of reaction was lowered to pH = 7 by adding appropriate amounts of HCl followed by quick filtration to prevent dissolution. Nitrogen atmosphere was constantly preserved on top of the solutions throughout the crystallization reactions to prevent intrusion of atmospheric carbon dioxide. The chemical speciation and activity based supersaturation were determined by thermodynamic calculation program Visual MINTEQ 3.1. The precipitates were collected at the end of each experiment by vacuum filtration through a 0.2 µm pore size filter (PP membranes). The ion concentrations in the filtrate were determined via spectrophotometry (Hach DR Lange 1900). The particle size distribution was performed and analyzed with Beckman Coulter LS230 laser diffraction particle size analyzer. The presented particle size distributions are based on dynamic light scattering technique and derived based on sphericity. Thus, the presented results are nominal size of crystals for the comparison of the results.

Solid phases were characterized via powder X-ray diffraction (XRD) (D8 Advance DaVinci, Bruker AXS GmBH) in the range of $5 - 75°$ with a step size of 0.013° and a step time of 0.67 s. The analysis of XRD data was performed by DIFRACC.SUITE EVA software (Bruker) and the International Centre for Diffraction Data database (ICDD PDF-4 + 2018) was used to characterize the precipitates. SEM analyses (Hitachi S-3400 N) were performed where samples were placed on carbon tape and sputter coated with gold. The zeta potential measurements were conducted by Malvern Zetasizer Nano ZS in a dip cell at 20 °C.

2.3. Design of experiments

The solution concentrations in this study were selected based on a dewatering reject of anaerobically digested sludge at a municipal wastewater treatment plant. The feed to the digester is a mixture of the thickened primary sludge and dewatered sludge that resulted from an enhanced biological phosphorus removal (EBPR) process. The operation strategy for supersaturation regulation is important in order to keep high recovery efficiency and product quality. The Mg:N:P = 1:1:1 is the theoretic requirement for struvite precipitation, while there is an imbalance between molar ratios of these ions in practical implications. The reagent cost for magnesium and alkali may affect the economic feasibility of struvite production [22]. In this work, different pH and Mg:N:P molar ratios were evaluated for struvite crystallization. The reaction kinetics at pH < 7.5 were very slow and pH > 9.5 may result in precipitation of other phases than struvite [23], thus the reaction pH were selected as pH = 7.5 (low), pH = 8.5 (medium) and pH = 9.5 (high). By combining different molar ratios with different pH values, struvite crystallization was investigated under a broad range of supersaturation and growth kinetics. The addition of magnesium beyond the consumption potential by struvite crystallization increases the operating cost, may result in formation of various magnesium phosphate precipitates and increases the chance of unintentional struvite precipitation in other processes [24]. Therefore, a series of preliminary experiments were performed to maximize P-recovery with minimum increment of Mg:P molar ratio beyond the stoichiometric value of 1:1. The Mg:P = 1.67:1 was selected based on the result of these experiments. The dewatering sidestreams of EBPR sludge both before and after anaerobic digestion are rich in phosphorus, while the reject flows after anaerobic digestion have significant surplus of ammonium with respect to phosphate and magnesium [25]. Therefore, the ammonium concentration to the crystallizer (N:P molar ratio) can be controlled by regulating the contribution of phosphate rich and ammonium rich streams or by control of recycle ratio of the reactor. According to technology providers N:P > 6 is optimal to maximize the recovery efficiency and purity of struvite and struvite precipitation would be of interest if N:P > 1 [19,26]. The molar ratio of N:P = 12 is the original N:P in the selected reject water and the other N:P molar ratios were selected based on these criteria. All experiments were performed in duplicates and Table 1 shows the experimental conditions and the thermodynamically calculated activity based supersaturation, S_a, for each experiment by using Eq. (1) [27]:

$$S_a = \left(\frac{IAP}{K_{sp}}\right)^{\left(\frac{1}{3}\right)} \qquad (1)$$

IAP = ion activity product = $a_{Mg^{2+}} \cdot a_{NH4^+} \cdot a_{PO4^{3-}}$
K_{sp} = thermodynamic solubility product
The thermodynamic equilibrium calculations for struvite

precipitation were performed by Visual MINTEQ 3.1 software to calculate the theoretical yield for each solution and the thermodynamic evaluation was followed by lab-scale batch experiments with a reaction duration of 60 min. The presented theoretical and experimental results of percent phosphorus recovery were calculated by using Eq. (2).

$$P- \text{ recovery }\% = \left(\frac{P_{initial} - P_{final}}{P_{initial}}\right) \times 100\% \qquad (2)$$

2.4. Preparation of solutions

Stock solutions of magnesium chloride hexahydrate ($MgCl_2 \cdot 6H_2O$), sodium dihydrogen phosphate ($NaH_2PO_4 \cdot 2H_2O$) and ammonium chloride (NH_4Cl) were prepared from their corresponding crystalline solids (Merck, reagent-grade) using MQ-water. Synthetic reject water was then prepared from the stock solutions following the original composition of the reject water with total ammonium nitrogen (NH_4-N = 745 mg/L) and total phosphate (PO_4-P = 137 mg/L) conforming N:P = 12:1, and the final composition in each experiment was adjusted to achieve the compositions in Table 1. The supersaturated solutions with respect to struvite were prepared by addition of the magnesium-containing solution to synthetic reject water under constant stirring.

2.5. Measurements of settling velocity

Sedimentation tests were conducted on an experimental set-up which was a modified form of the Andreasen pipette method [28]. The set-up consisted of a cylindrical glass burette with 8 mm internal diameter filled with water pre-saturated with respect to struvite to avoid dissolution. The sieved crystals were dispersed in 1 mL of the same liquid and allowed to make a distinct front before measurements. The measuring system was based on visual space-time registration and travel time of the particles measured by digital-display stopwatch.

3. Results and discussion

3.1. Efficiency of phosphorus recovery

The initial phosphorus concentration is equal in all conditions and the final phosphorus concentration is determined by the solubility of struvite, which is constant at constant temperature, for the calculation of theoretical yield. Fig. 1 presents the experimentally measured and theoretically percent P-recovery values for all determined conditions. The increasing values of P-recovery shown with thermodynamic calculations reflect the effect of higher supersaturation in the reaction medium that is achieved either by increasing the pH or molar ratio of the constituent ions with respect to P. The results for struvite yield
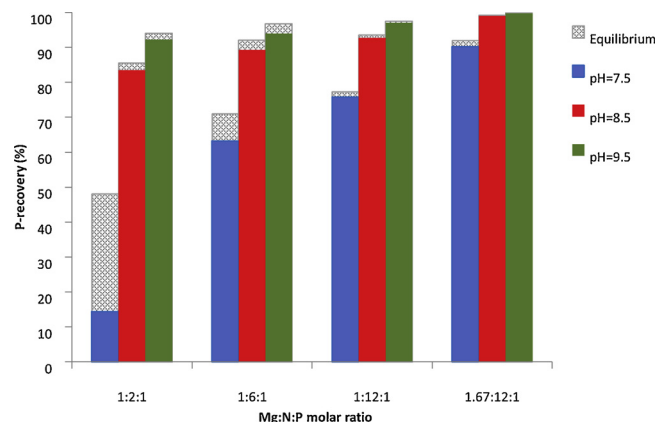
Table 1
Experimental conditions and calculated activity based supersaturation values (P = 137 mgL^{-1}).

ExP.	Mg:N:P	pH	Sa
1	1:2:1	7.5	1.5
2	1:2:1	8.5	3.3
3	1:2:1	9.5	5.8
4	1:6:1	7.5	2.1
5	1:6:1	8.5	4.5
6	1:6:1	9.5	7.9
7	1:12:1	7.5	2.4
8	1:12:1	8.5	5.3
9	1:12:1	9.5	9.5
10	1.67:12:1	7.5	2.7
11	1.67:12:1	8.5	5.9
12	1.67:12:1	9.5	10.6

Fig. 1. The P-recovery measured in the experiments and equilibrium theoretical P-recovery calculated from Visual MINTEQ.

based on thermodynamic equilibrium calculation are presented in Figure S1.

The strong influence of pH on supersaturation results from its deterministic effect on phosphate and ammonia speciation in solution (Table S1) [60]. Increasing pH shifts the equilibrium reactions of struvite constituents, which consequently increases the supersaturation with respect to struvite. A satisfactory fit was observed between theoretical and experimental results within the reaction time of 60 min determined for this study, except for two sets of experiments at pH = 7.5 with lowest supersaturation values due to slower reaction kinetics (Mg:N:P = 1:6:1 and Mg:N:P = 1:2:1). Higher supersaturation means a higher chemical potential for the crystallization of struvite and consequently a higher phosphorus recovery as observed in the thermodynamic calculations. Increasing Mg:P and N:P molar ratio at low pH (7.5) caused a greater effect on P-recovery efficiency than that in higher pH values.

Moreover, experimental results also showed the strong effect of supersaturation on the kinetics of the precipitation reaction and indicated that supersaturation is a key parameter for efficient P-recovery by precipitation. Both nucleation and crystal growth rates scale with supersaturation, thus, the reaction times for completing the precipitation shorten under high supersaturation. The rate of NaOH addition for maintaining the solution pH during the precipitation reactions was an indication of the reaction progression [22] and it was found that among the studied factors, pH showed the major effect on the reaction time. Increasing the reaction pH from 7.5 to 8.5 and from 8.5 to 9.5, reduced the time for completing the reactions by a factor of ≈ 5 and ≈ 3, respectively (data not shown). According to the results of ion and complex speciation by Visual MINTEQ 3.1 (Figure S2) the increase of pH changes the ion speciation and ion complexations towards a higher PO_4^{3-} and $MgPO_4^-$ content while decreasing free Mg^{2+} and NH_4^+. This implies that higher rates of the precipitation reactions at higher pH can mainly be explained based on higher amounts of available phosphate precursors. This hypothesis is in line with the findings of Abbona et al. deducted from molecular modeling based on periodic bond chain (PBC) theory [8].

The slow reaction kinetics observed at low supersaturation levels can be disadvantageous in the case of full-scale application specially for big treatment plants with high flows of reject water. Therefore, supersaturation adjustment via pH and precursor concentration is of vital importance for enhanced recovery efficiency. The struvite rectors must be optimized to not only convert the soluble phosphorus to struvite but also to maximize the quality and collection of the product [29]. However, the dissimilarities associated with reactor type (i.e. fluidized bed, air-agitated and stirred) make this optimization challenging. Aeration is mainly practiced for pH increase by CO_2 stripping, while process regulation by aeration adjustment could be challenging due to complex dependency of turbulence on bubble size and reactor dimensions. Further, it has been reported that adjustment of aeration intensity did not improved the struvite recovery and particle settling [30]. In stirred reactors, the mixing improvement enhances the struvite recovery by more homogenous distribution of supersaturation and preventing local peaks in supersaturation, otherwise mixing by itself can not be considered as the main parameter for optimization. Therefore, process optimization requires selection of a proper control parameter. Supersaturation incorporates the impact of essential parameters (constituent ions, pH and temperature) and has the privilege to uncouple the optimization to a great extent from reactor type. Moreover, supersaturation regulation approach can be further utilized for crystal growth and kinetics studies as a well-established theoretical and practical knowledge is available on the supersaturation role in different aspects of crystallization process [10,27,31].

3.2. Product characterization: purity and crystal morphology

In the crystallization systems with sufficient concentrations of

Mg^{2+}, NH_4^+ and PO_4^{3-} ions, struvite and various magnesium phosphate minerals can potentially precipitate. However, the final precipitate is the result of both thermodynamic and reactions kinetics. The thermodynamic calculations showed that at the defined experimental conditions, the supersaturated phases were limited to struvite, newberyite ($MgHPO_4 \cdot 3H_2O$) and trimagnesium phosphate ($Mg_3(PO_4)_2$).

The intensity and positions of XRD patterns matched with the reference powder diffraction file for struvite (PDF 00-015-0762) that further confirmed presence of pure struvite under all experimental conditions (Figure S3). Further, based on defined experimental conditions, obtaining pure struvite is in accordance with previous studies. It is reported that nucleation rate of struvite is greater than that of newberyite and newbryite is the stable form at low pH (pH < 6) and high magnesium concentrations [32]. Trimagnesium phosphate has never been observed in the pH range of 6–9.5 and is reported to have low precipitation rate. Therefore, in the pH range of this work, neither newberyite nor trimagnesium phosphate are kinetically favorable phases and struvite precipitation is more abundant [23,32,33].

The morphology (external shape) of a crystalline particle is determined by the intrinsic characteristics of the crystal structure and the external factors of growth conditions such as solution composition and temperature. The final crystal morphology arises as a result of the relative growth rates of each of its faces which are affected by both internal and external elements of growth [24,34]. Fig. 2 shows the wedge shape morphology of struvite crystals with corresponding miller indices for different faces.

The effects of reaction conditions on the final crystal morphology are investigated in detail and Fig. 3 summarizes the different morphologies observed at varying conditions of supersaturation and ammonium concentration. The represented morphologies in Fig. 3 are selected after thorough inspection by SEM in order to report the dominant crystal morphology in each experiment. The observed morphologies are categorized in three groups as polyhedral (well-faceted), hopper and rough (dendritic) morphologies with a possible transition boundary between them.

3.2.1. Effects of supersaturation on struvite morphology

Struvite morphologies observed at low supersaturations ($S_a = 1$–3) showed a well-faceted structure with a bipyramidal appearance and generally free of major defects (zone 1). The crystals at $S_a = 1.5$ (Fig. 3a) reflected the most basic morphology of struvite crystal that is hemimorphic with unequally developed [001] and [00$\bar{1}$] faces. In this zone, increasing the ammonium concentration triggered the growth of [001] face which appeared as a sharp and narrow face on the top of the crystal (Fig. 3b, c and d). It can be seen that in zone 1 increasing pH by one unit caused longitudinal elongation of the crystals (Fig. 3e). Increasing the supersaturation beyond $S_a = 3$, either by increasing the pH or the concentration of constituent ions, initiated the transition between zone 1 with well-faceted crystals and zone 2 with hopper crystals. The crystals observed in zone 2 seemed to be twin crystals with the
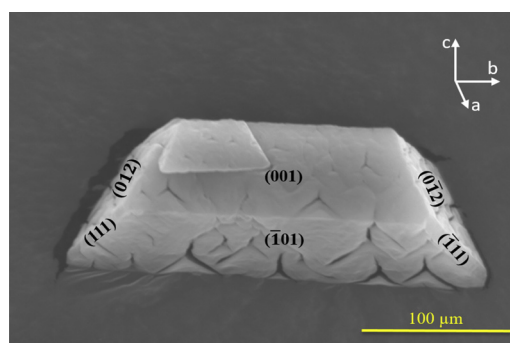

Fig. 2. The wedge shape morphology of struvite crystals. The facets are defined with corresponding Miller indices.
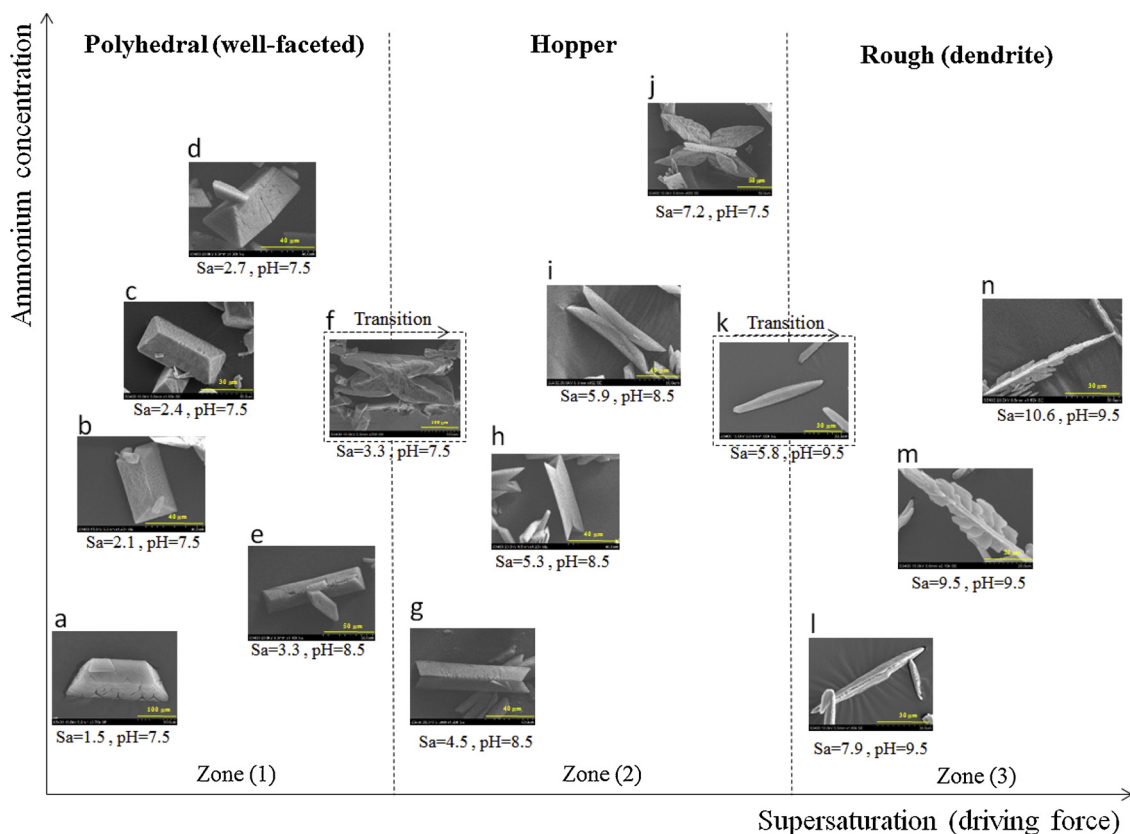
Fig. 3. Crossover of the struvite morphology versus activity based supersaturation and ammonium concentration (note that the placement of f and k do not follow the placement with respect to axes).

X-shape morphology. It was noticed that as the supersaturation was increased, the area of the [012] planes became smaller and it eventually disappeared at higher supersaturation. The further increase of supersaturation resulted in the formation of needle-like and dendritic crystals with high aspect ratios as shown in zone 3. It was observed that higher levels of supersaturation attained by increasing the ammonium concentration within zone 3 amplified the branching of struvite crystals and shifted the needle-like morphology to a dendrite. (Fig. 3m, n).

The transition exhibited by the crystals from polyhedral to dendritic morphologies was induced by changing growth mechanisms as a result of the increasing supersaturation. Under low to moderate supersaturation levels growth is surface reaction controlled and monocrystalline particles with polyhedral morphologies are the expected outcomes of the advancement of smooth faces along the crystal lattice. With increasing driving force, surface roughness increases due to extensive surface nucleation and stimulates a change in the growth mechanism from reaction-controlled to diffusion-controlled growth. The diffusion field around crystals becomes prominent on their development under these conditions and concentration gradients along the diffusion field induce morphological instabilities at the crystal interface. Depending on the diffusion field, certain edges and corners of crystals can have access to higher supersaturation and consumption of supersaturation by growth of these locations prevents growth of the central part, which results in hopper crystals (Fig. 4a) [31]. Further elevation of the characteristics observed in hopper crystals results in a more efficacious advancement in the direction of high supersaturation along the same lattice and give rise to dendritic growth. The X-shape morphology can be considered as an intermediate stage of evolution between the well-faceted and dendrite crystals or as an implicit boundary between slow and rapid growth (Fig. 3) [35,36].

Previous studies also showed that the internal structure of struvite induces surfaces with higher potential and probability of growth in
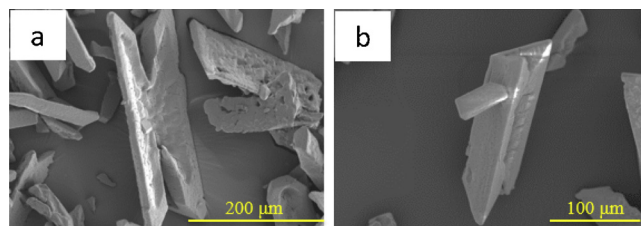

Fig. 4. The X-shape morphology of struvite crystals from a) bottom and b) side views.

certain directions, which will regulate the final morphology of struvite crystals [8]. However, the complex morphology of X-shape crystals has been explained by some researchers to be formed by self-assembly and fusion of independent crystals [37–39]. In order to investigate this hypothesis, crystallization reactions with different initial supersaturation values were terminated at varying time intervals and precipitates were examined by SEM (Fig. 4). Our results did not show any supporting evidence for mesocrystal formation, which proposes that a composite structure forms via oriented aggregation of small particles [36]. Instead, we suggest these complex morphologies are mainly surface patterns that reflect different shapes due to different growth rates of struvite faces. However, further interpretations cannot be made within the scope of this work and detailed investigations would be necessary to determine the underlying formation mechanism of these morphologies.

From practical point of view, the regulation of supersaturation is achievable by adjustment of the nutrient rich flows, chemical dosing and pH. Although, the accurate measurement of supersaturation in full-scale applications is quiet challenging since the real wastewater is a complex matrix of organic and inorganic materials [40]. The crystal morphology yet can be determined by simple microscopy or an image

analysis technique, which further can be used as an auxiliary indicator for approximation of the supersaturation extent (Fig. 3).

3.2.2. Effects of Mg^{2+} and NH_4^+ concentration

The effect of Mg^{2+} on struvite morphology was mainly observed as a regulator of supersaturation and reaction kinetics. The reflection of higher Mg^{2+} concentration on the morphology of crystal is observed in the development of [00ī] face. The higher Mg^{2+} concentration slightly increased the longitudinal elongation of crystals along b-axis (Fig. 3c, 3d and 3h, 3i). This is in line with the molecular modeling and previous observations in other studies [36,37].

The ammonium concentration influences the lateral growth and thickness of struvite crystals (Fig. 3a, c and c, d). This deduction is based on several experiments in addition to presented experiments in this paper and it will be discussed in more detail. Struvite crystals consist of tetrahedral PO_4^{3-} and NH_4^+, and $Mg[H_2O]_6^{2+}$ species. In all observed morphologies the [00ī] face is larger than [001] face and NH_4^+ concentration is efficient in shaping the outcrop of [00i] surfaces (i = 1–4) (Fig. 3). For moderately low values of pH (about 7.5) and low concentrations of NH_4^+, the [001] face appears as a flat trapezoidal surface which is elongated more along b-axis (Fig. 2). Higher concentrations of NH_4^+ produced a sharp outcrop for this face and it triggered the growth of [00i] (i = 1–4) faces. At medium pH = 8.5 the lower concentration of NH_4^+ hindered the formation of a smooth finished surface at [001] face and at high pH = 9.5 it can be seen that the higher concentrations of NH_4^+ induced the dendritic structure of the crystals which has started on the top face of [001] (Fig. 3). However, lower concentrations of NH_4^+ resulted in smoother top surface and less branching of crystals.

It has previously been reported that the [001] surface has the higher density of electropositive groups (NH_4^+) or in other words the NH_4^+ groups terminate the [001] surface [41]. PO_4^{3-} and $Mg[H_2O]_6^{2+}$ groups terminate the [00ī] surface that makes the c-axis a dipole axis [36,41]. Thus, increasing the content of NH_4^+ affects the distribution of supersaturation around the growing crystal. The NH_4^+ groups on [001] faces are likely to be more polarized than the PO_4^{3-} and $Mg[H_2O]_6^{2+}$ groups on [00ī] face [41]. The NH_4^+ groups can induce growth along the c-axis and outcrop on [00i] surface (i = 1–4) that results in such structures. The XRD results (Figure S3) further showed that the expression of observed peaks for [002] (2θ = 15.78) and [004] (2θ = 31.88) were higher in the case of higher NH_4^+ concentration.

3.3. Product properties

3.3.1. Size distribution

The final particle size, purity and crystal morphology are the key factors to the phosphorus recovery efficiency [42]. The desired size of struvite particles mostly depends on its final use. Smaller particles have higher release rate of nutrients because of their high surface area/volume ratio [43,44]. However, in the nutrient recovery by struvite crystallization, uniform distribution of big particles with minimum contribution of fine particles is favorable. Bigger particles settle faster and bring less challenge in post-handling like drying and filtration, while the fine particles increase the chance of wash out from the reactor, especially in fluidized bed reactors (FBR) [29,45].

Fig. 5 presents the nominal size distribution graphs for struvite particles precipitated at different conditions. As a general trend, the particle size decreased with increasing initial supersaturation and a more homogenous size distribution was obtained for the particles crystallized at lower supersaturations. The particle sizes were in the range of 70–90 μm in zone 1, 40–60 μm in zone 2 and 20–50 μm in zone 3.

The share of fine particles (smaller than 10 μm) in final products were also calculated at each experimental condition and given in Fig. 6. Results show that the share of fine particles increased with increasing

supersaturation via both pH and ion concentrations. Experiments conducted at pH = 7.5 had no share of fine particles except for the lowest supersaturation condition at the case of Mg:N:P = 1:2:1. As shown in Fig. 1, 60 min reaction time was not enough for complete growth of crystals at that supersaturation (S_a = 1.5) which resulted in fine particle formation in this case.

Supersaturation is the main driving force for the crystallization process and highly influences particle size and size distribution due to its strong effect on the nucleation rate. Smaller particles observed with increasing initial supersaturation results from boosted nucleation rates that produces higher number of particles, which then consume the remaining supersaturation by crystal growth [10]. Similarly, the increasing share of fine particles detected at pH = 8.5 and pH = 9.5 is associated with high initial supersaturation which implies high nucleation rate [46]. Thus, lower initial supersaturation levels that result in large size crystals with a lower content of fine particles can be considered for process optimization.

3.3.2. Settleability

Crystal size and shape affect the efficiency of downstream processes like settleability, filtering and drying, so it is important to be able to tailor process conditions for optimization of these properties. Improving crystal settleability by optimization of reaction parameters to minimize loss of crystals due to wash out will enhance phosphorus recovery efficiency and ensure the quality of effluent [47].

There are different factors that affect the settling velocity of a particle like size, shape and density [48]. The settleability test was performed on the varying morphologies of struvite particles that were obtained at different reaction conditions. Sieving was used in order to investigate the effects of size and morphology separately on the settling velocity of struvite particles. Fig. 7 shows the results of statistical analysis for these measurements.

Results showed the strong dependency of the settling velocity on both size and morphology of the precipitates. The bigger crystals settled faster for all morphologies. Among different morphologies, the bipyramidal crystals had the highest settling velocity for all crystal sizes followed by X-shape crystals and the lowest settling velocity was observed for the dendritic (needle-shape) crystals. The difference of the settling velocities can be explained based on difference in mass and packing density of the particles [49]. Further, the needle-shaped crystals with high aspect ratio do not favor proper settling due to the higher drag force they experience, which might cause difficulties during settling and filtration [50].

These results reveal that for a more efficient solid-liquid separation and better settling properties, the struvite particles crystallized under low to moderate supersaturation conditions can be advantageous.

3.3.3. Aggregation

During crystallization, particles may grow as single particles or in aggregates. The aggregation of struvite crystals is favorable for wastewater applications since bigger aggregates settle faster and mediate the granulation in the reactor. It is reported that the higher structural strength of struvite pellets can be achieved by aggregation of fine struvite crystals [51].

The aggregation process affects the final particle size and it requires collision of particles and a sufficient period that particles stay together [52]. Previous research has shown that supersaturation affects the aggregation of struvite particles by influencing the adherence of particles and increasing the pH of the precipitation reaction leads to the production of particles with weak aggregation and settling properties [16,53]. In our study, we also observed that both pH and supersaturation are important parameters for aggregation of struvite particles. Fig. 8 shows SEM images of struvite crystal with stronger aggregation at low values of initial supersaturation and reaction pH (a, b and c), and their transition to weak aggregates and to single crystals (d, e and f) with increasing values of these parameters. In general, results
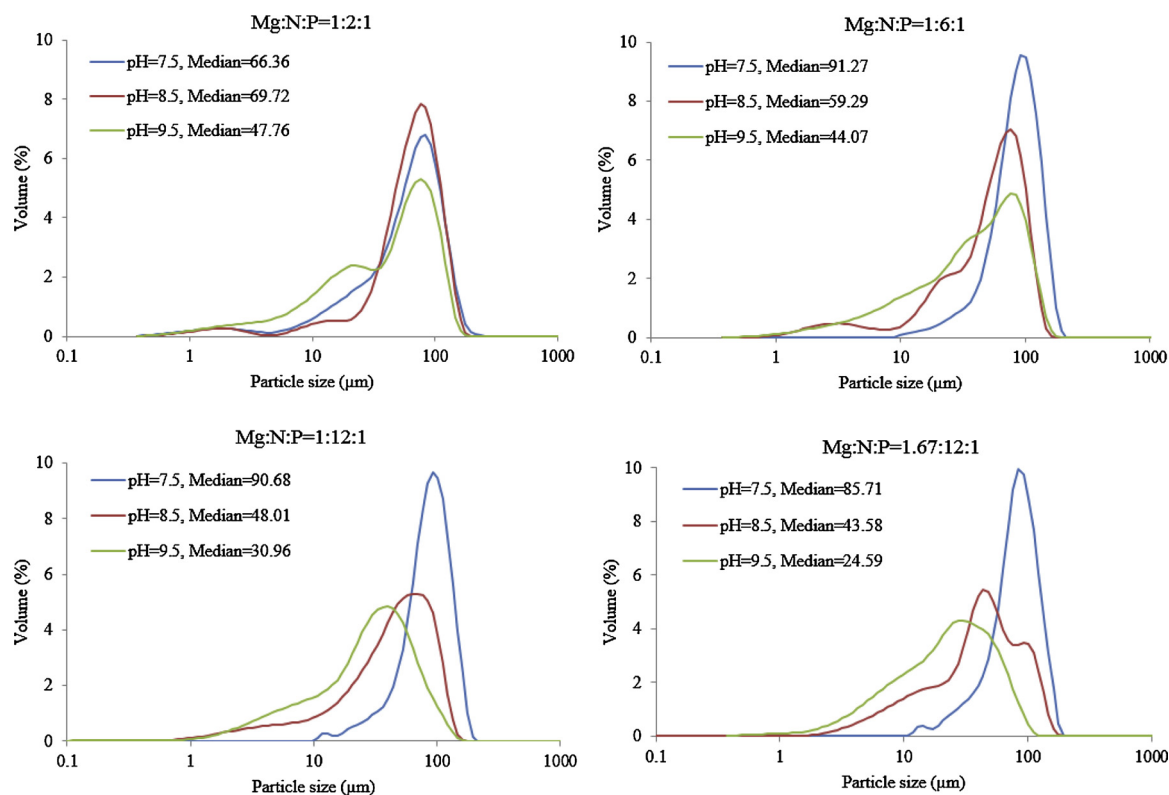
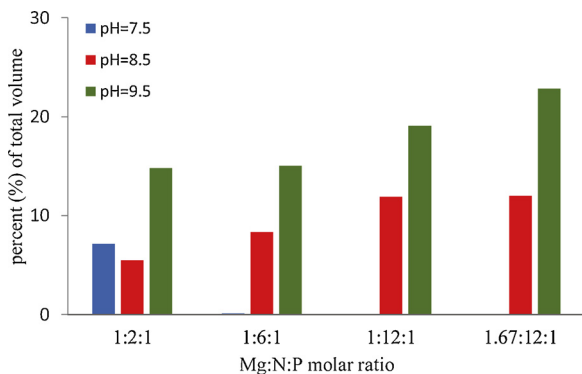**Fig. 5.** Particle size distribution for struvite particles precipitated at different conditions.

Fig. 6. The share of fine particles (< 10 μm) by volume percent in the final products precipitated at different experimental conditions.
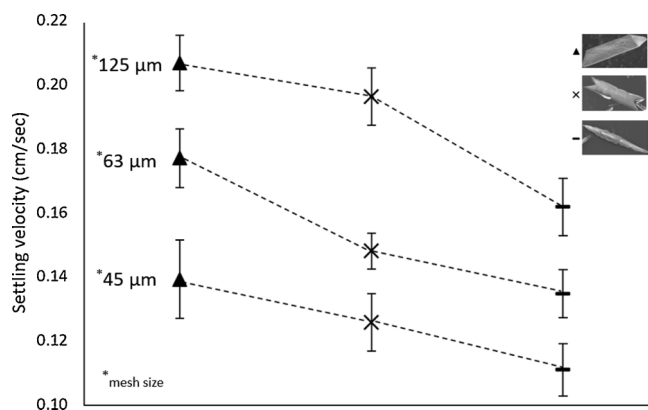

Fig. 7. The settling velocity of struvite particles with different size and morphologies (bars show standard deviations).

showed that struvite particles crystallized under conditions corresponding to zone 1 (Fig. 3) displayed better aggregation properties.

The measured zeta potentials for crystals at Mg:N:P = 1:12:1 and in different pH levels (ζ = -7.51 mV at pH = 7.5, ζ = -9.30 mV at pH = 8.5 and ζ = -17.06 mV at pH = 9.5) confirmed that struvite particles have higher negative zeta potential at higher pH values. It is known that the aggregation of particles is mainly governed by surface charge and struvite crystals showed higher negative surface charge at higher pH values, which disrupts the aggregation potential and settleability due to increased repulsive forces [18,54,55]. Therefore, crystallization reactions held at low pH can mediate stronger charge induced aggregates of struvite crystals termed as micro flocs that can initiate the formation of compact aggregates by adsorption and bridging in the case of sufficient supersaturation. The aggregation of micro flocs is an important step that affects the efficiency of solid/liquid separation [56]. As shown in Fig. 8e and f, when pH was increased to 9.5, no aggregation was observed due to the high negative zeta potential of crystals precipitated under this pH value.

Our results also showed the influence of initial supersaturation on the aggregative properties along with the reaction pH. The comparison of Fig. 8c and d (corresponding to Fig. 3e and g, respectively) showed better aggregated struvite crystals in the zone 1. Aggregation rate shows a linear relationship with crystal growth rate and scales with supersaturation [57]. Thus, maintaining sufficiently high levels of supersaturation during growth of particles can enhance their aggregation. Zone 1 lies low in the supersaturation scale of our experiments; however, in this work only the initial values of supersaturation are determined. High initial supersaturation induces high nucleation rates and generation of higher numbers of particles, which triggers faster consumption of supersaturation during growth regime. On the contrary, the low initial supersaturation in zone 1 implies maintaining of supersaturation for longer time during growth; hence, particle aggregation is improved.

The aggregation of struvite particles has practical implications since it favors the round granular shape of struvite. The granular struvite
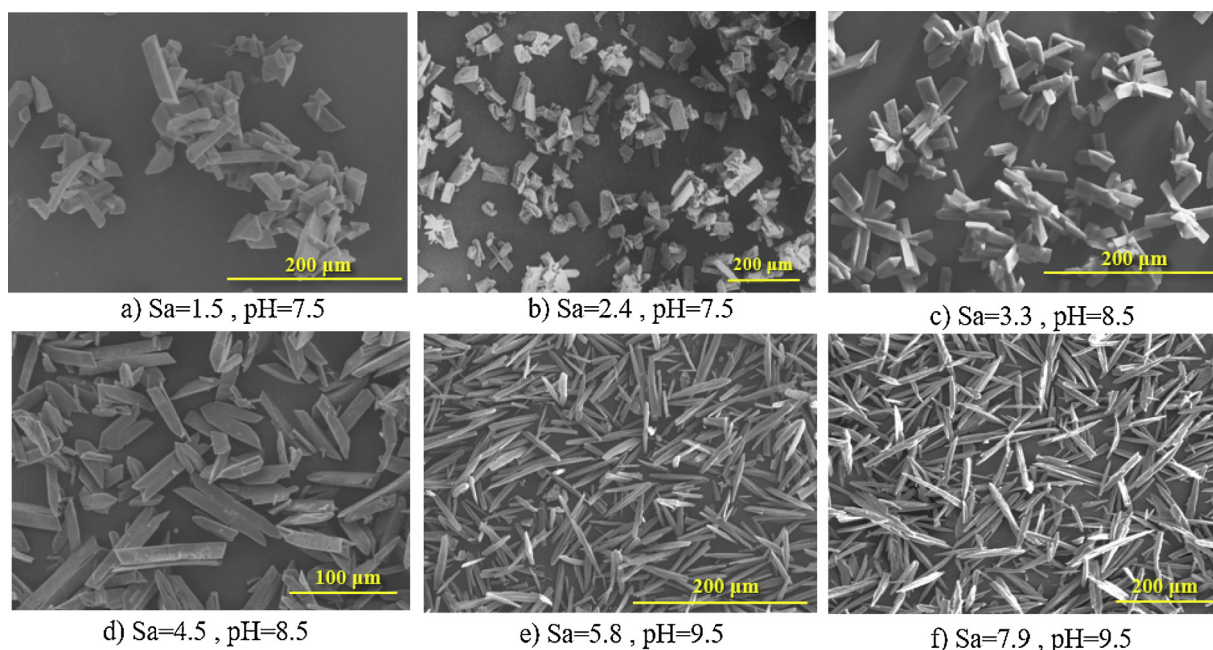
a) Sa=1.5 , pH=7.5   b) Sa=2.4 , pH=7.5   c) Sa=3.3 , pH=8.5

d) Sa=4.5 , pH=8.5   e) Sa=5.8 , pH=9.5   f) Sa=7.9 , pH=9.5

Fig. 8. a, b and c) stronger aggregation of struvite crystal at low supersaturation, d, e and f) weak aggregates of struvite crystals and single crystals at higher supersaturation.

particles are preferable for ease of transportation and its applicability to the farmers' spreading equipment [58]. It was also reported that X-shape struvite crystals do not favor the production of struvite granules, which is undesired for agriculture purposes [59].

The results of this study show that struvite crystals precipitated at different reaction conditions have different aggregation properties. The electric charge of crystals plays an important role in granulation and particle-particle interactions, and solution pH is shown to be an effective parameter for its control [15]. Solution supersaturation is another important factor, where continuous measurement can impose some practical difficulties for full-scale applications; however, adjustment of initial values can be utilized for successful granulation.

4. Conclusion

Variational digester supernatant composition and operating conditions in wastewater treatment plants requires adjustment of operating parameters to ensure high P-recovery efficiency and product quality. This study presents how different concentrations of struvite constituents (Mg^{2+}, NH_4^+) and pH affect phosphorus recovery along with crystal size and morphology, and settling and aggregation properties of the final products.

It is concluded that an integrated optimization of both recovery efficiency and product properties (size, aggregation and settling) is necessary to achieve a well-controlled struvite crystallization. The supersaturation regulation is an effective approach to define the operational window for this integrated optimization. The proper control of supersaturation through controlling the pH and ion concentrations in the reaction medium demonstrated the combined effects of operating conditions and feed composition on the final properties of the struvite crystals. The operational conditions for production of three dominant struvite morphologies are presented and the recovery potential and properties of final crystals are discussed at each experimental condition. In brief, providing the operational condition in a way that it lies in zone 1 (Fig. 3) produced bigger crystalline particles with better settling and aggregation properties than zone 2 (Fig. 3) and the dendritic crystals in zone 3 (Fig. 3) were not favorable in terms of settleability and aggregative properties. Moreover, maintaining the sufficient levels of supersaturation after nucleation showed improved aggregation of

struvite crystals. These results revealed that product properties, like crystal size and morphology, can be efficiently controlled by supersaturation. On the other hand, the general trend of phosphorus recovery did not follow the same trend where the efficiency was highest in zone 3 with high supersaturation values.

The overall process efficiency requires maximized phosphorus recovery and favorable product properties. The results of this study show that the supersaturation regulation is an effective strategy to optimize the recovery efficiency and to consistently attain the desired struvite properties.

Notes

The authors declare no competing financial interest.

Appendix A. Supplementary data

Supplementary material related to this article can be found, in the online version, at doi:https://doi.org/10.1016/j.jece.2019.102918.

References

[1] L. Vasenko, H. Qu, Novel two-stage oxidation/crystallization technology for high-purity calcium phosphates recovery from digester supernatant, J. Environ. Chem. Eng. 6 (2018) 2975–2982, https://doi.org/10.1016/j.jece.2018.04.051.
[2] Y. Luo, H. Li, Y.R. Huang, T.L. Zhao, Q.Z. Yao, S.Q. Fu, G.T. Zhou, Bacterial mineralization of struvite using MgO as magnesium source and its potential for nutrient recovery, Chem. Eng. J. 351 (2018) 195–202, https://doi.org/10.1016/j.cej.2018.06.106.
[3] M.R. Gaterell, R. Gay, R. Wilson, R.J. Gochin, J.N. Lester, An economic and environmental evaluation of the opportunities for substituting phosphorus recovered from wastewater treatment works in existing uk fertiliser markets, Environ. Technol. 21 (2000) 1067–1084, https://doi.org/10.1080/09593332108618050.
[4] V. Oliveira, J. Labrincha, C. Dias-Ferreira, Extraction of phosphorus and struvite production from the anaerobically digested organic fraction of municipal solid waste, J. Environ. Chem. Eng. 6 (2018) 2837–2845, https://doi.org/10.1016/j.jece.

2018.04.034.

[5] J.D. Doyle, S.A. Parsons, Struvite formation, control and recovery, Water Res. 36 (2002) 3925–3940, https://doi.org/10.1016/S0043-1354(02)00126-4.

[6] M.I.H. Bhuiyan, Investigation Into Struvite Solubility, Growth and Dissolution Kinetics in the Context of Phosphorus Recovery from Wastewater, (2007), p. 212.

[7] S. Agrawal, J.S. Guest, R.D. Cusick, Elucidating the impacts of initial supersaturation and seed crystal loading on struvite precipitation kinetics, fines production, and crystal growth, Water Res. 132 (2018) 252–259, https://doi.org/10.1016/j.watres.2018.01.002.

[8] F. Abbona, R. Boistelle, Growth morphology and crystal habit of struvite crystals (MgNH4PO4·6H2O), J. Cryst. Growth 46 (1979) 339–354, https://doi.org/10.1016/0022-0248(79)90082-4.

[9] N. Marti, A. Bouzas, A. Seco, J. Ferrer, Struvite precipitation assessment in anaerobic digestion processes, Chem. Eng. J. 141 (2008) 67–74, https://doi.org/10.1016/j.cej.2007.10.023.

[10] C.M. Mehta, D.J. Batstone, Nucleation and growth kinetics of struvite crystallization, Water Res. 47 (2013) 2890–2900, https://doi.org/10.1016/j.watres.2013.03.007.

[11] G.D.B.P. Dudley, Springer Handbook of Crystal Growth, Springer Berlin Heidelberg, Berlin, Heidelberg, 2010, https://doi.org/10.2465/gkk.39.193a.

[12] S.L. Price, Is zeroth order crystal structure prediction (CSP_0) coming to maturity? What should we aim for in an ideal crystal structure prediction code? Faraday Discuss. 211 (2018) 9–30, https://doi.org/10.1039/c8fd00121a.

[13] B.K.N. Ohlinger, S. Member, T.M. Young, A. Member, E.D. Schroeder, K.N. Ohlinger, Kinetics effects on preferential struvite accumulation in wastewater, J. Environ. Eng. 125 (1999) 730–737, https://doi.org/10.1061/(ASCE)0733-9372(1999)125:8(730).

[14] H. Huang, D.S. Mavinic, K.V. Lo, F.A. Koch, Production and basic morphology of struvite crystals from a pilot-scale crystallization process, Environ. Technol. 27 (2006) 233–245, https://doi.org/10.1080/09593332708618637.

[15] N.C. Bouropoulos, P.G. Koutsoukos, Spontaneous precipitation of struvite from aqueous solutions, J. Cryst. Growth 213 (2000) 381–388, https://doi.org/10.1016/S0022-0248(00)00351-1.

[16] Z. Ye, Y. Shen, X. Ye, Z. Zhang, S. Chen, J. Shi, Phosphorus recovery from wastewater by struvite crystallization: property of aggregates, J. Environ. Sci. China (China) 26 (2014) 991–1000, https://doi.org/10.1016/S1001-0742(13)60536-7.

[17] S. Kataki, H. West, M. Clarke, D.C. Baruah, Phosphorus recovery as struvite from farm, municipal and industrial waste: feedstock suitability, methods and pretreatments, Waste Manage. 49 (2016) 437–454, https://doi.org/10.1016/j.wasman.2016.01.003.

[18] A.N. Kofina, P.G. Koutsoukos, Spontaneous precipitation of struvite from synthetic wastewater solutions, Cryst. Growth Des. 5 (2005) 489–496, https://doi.org/10.1021/cg049803e.

[19] K.S. Le Corre, E. Valsami-Jones, P. Hobbs, B. Jefferson, S.A. Parsons, Struvite crystallisation and recovery using a stainless steel structure as a seed material, Water Res. 41 (2007) 2449–2456, https://doi.org/10.1016/j.watres.2007.03.002.

[20] N.Ö. Yigit, S. Mazlum, Phosphate recovery potential from wastewater by chemical precipitation at batch conditions, Environ. Technol. 28 (2007) 83–93, https://doi.org/10.1080/09593332808618768.

[21] O. Tünay, I. Kabdasli, D. Orhon, S. Kolçak, Ammonia removal by magnesium ammonium phosphate precipitation in industrial wastewaters, Water Sci. Technol. 36 (1997) 225–228, https://doi.org/10.1016/S0273-1223(97)00391-0.

[22] E. Heraldy, F. Rahmawati, H. Heriyanto, D.P. Putra, Preparation of struvite from desalination waste, J. Environ. Chem. Eng. 5 (2017) 1666–1675, https://doi.org/10.1016/j.jece.2017.03.005.

[23] V. Babić-Ivančić, J. Kontrec, L. Brečević, D. Kralj, Kinetics of struvite to newberyite transformation in the precipitation system MgCl2-NH4H2PO4-NaOH-H2O, Water Res. 40 (2006) 3447–3455, https://doi.org/10.1016/j.watres.2006.07.026.

[24] A. Adnan, D.S. Mavinic, F.A. Koch, Pilot-scale study of phosphorus recovery through struvite crystallization- examining the process feasibility, J. Environ. Eng. Sci. 2 (2003) 315–324, https://doi.org/10.1139/s03-040.

[25] S. Shaddel, S. Ucar, J.-P. Andreassen, S.W. Østerhus, Enhancing efficiency and economy of phosphorus recovery process by customizing the product based on sidestream characteristics, Proc. IWA Nutr. Remov. Recover. Conf. 2018 (2018).

[26] C. Vaneeckhaute, E. Belia, J. Copp, E. Meers, F. Tack, P. Vanrolleghem, Roadmap for setting up optimal treatment trains for nutrient recovery at WRRFs, Proc. Water Environ. Fed. 2017 (2017) 522–528, https://doi.org/10.2175/193864717821494529.

[27] J.W. Mullin, Crystallization, Butterworth-Heinemann, (2001).

[28] R.W. Farmer, J.R. Beckman, Particle Size Distribution Analysis of Blended Solids by a Modified Andreasen Pipet Method, Ind. Eng. Chem. Process Des. Dev. 23 (1984) 341–343, https://doi.org/10.1021/i200025a027.

[29] A. Grooms, S. Reusser, A. Dose, A. Britton, R. Prasad, Operating experience with ostara struvite harvesting process, Proc. Water Environ. Fed. 2015 (2015) 2162–2177, https://doi.org/10.2175/193864715819538651.

[30] W. de Buck, Struvite Crystallization and Separation in Digested Sludge, (2012).

[31] J.-P. Andreassen, A.E. Lewis, Classical and nonclassical theories of crystal growth, New Perspect. Miner. Nucleation Growth, Springer International Publishing, Cham, 2017, pp. 137–154, https://doi.org/10.1007/978-3-319-45669-0_7.

[32] M. Türker, I. Çelen, Chemical equilibrium model of struvite precipitation from anaerobic digester effluents, Turk. J. Eng. Environ. Sci. 35 (2011) 39–48, https://doi.org/10.3906/muh-1008-15.

[33] J.D. Doyle, S.A. Parsons, Struvite formation, control and recovery, Water Res. 36 (2002) 3925–3940, https://doi.org/10.1016/S0043-1354(02)00126-4.

[34] H. Takiyama, Supersaturation operation for quality control of crystalline particles

[35] M. Daudon, D. Bazin, G. André, P. Jungers, A. Cousson, P. Chevallier, E. Véron, G. Matzen, Examination of whewellite kidney stones by scanning electron microscopy and powder neutron diffraction techniques, J. Appl. Crystallogr. 42 (2009) 109–115, https://doi.org/10.1107/S0021889808041277.

[36] J. Prywer, A. Torzewska, T. Plociński, Unique surface and internal structure of struvite crystals formed by Proteus mirabilis, Urol. Res. 40 (2012) 699–707, https://doi.org/10.1007/s00240-012-0501-3.

[37] H. Li, Q.Z. Yao, Y.Y. Wang, Y.L. Li, G.T. Zhou, Biomimetic synthesis of struvite with biogenic morphology and implication for pathological biomineralization, Sci. Rep. 5 (2015) 1–8, https://doi.org/10.1038/srep07718.

[38] D. Bazin, G. André, R. Weil, G. Matzen, V. Emmanuel, X. Carpentier, M. Daudon, Absence of bacterial imprints on struvite-containing kidney stones: a structural investigation at the mesoscopic and atomic scale, Urology 79 (2012) 786–790, https://doi.org/10.1016/j.urology.2011.08.054.

[39] L. Chen, Y. Shen, A. Xie, F. Huang, W. Zhang, S. Liu, Seed-mediated synthesis of unusual struvite hierarchical superstructures using bacterium, Cryst. Growth Des. 10 (2010) 2073–2082, https://doi.org/10.1021/cg900974n.

[40] X. Ye, Y. Gao, J. Cheng, D. Chu, Z.L. Ye, S. Chen, Numerical simulation of struvite crystallization in fluidized bed reactor, Chem. Eng. Sci. 176 (2018) 242–253, https://doi.org/10.1016/j.ces.2017.10.048.

[41] F. Abbona, M. Calleri, G. Ivaldi, Synthetic struvite, MgNH4PO4.6H2O: correct polarity and surface features of some complementary forms, Acta Crystallogr. Sect. B 40 (1984) 223–227, https://doi.org/10.1107/S0108768184002020.

[42] D.S. Perwitasari, S. Muryanto, J. Jamari, A.P. Bayuseno, Kinetics and morphology analysis of struvite precipitated from aqueous solution under the influence of heavy metals: Cu2+, Pb2+, Zn2+, J. Environ. Chem. Eng. 6 (2018) 37–43, https://doi.org/10.1016/j.jece.2017.11.052.

[43] A.L. Forrest, K.P. Fattah, D.S. Mavinic, F.A. Koch, Optimizing struvite production for phosphate recovery in WWTP, J. Environ. Eng. New York (New York) 134 (2008) 395–402, https://doi.org/10.1061/(ASCE)0733-9372(2008)134:5(395).

[44] T.H. Muster, G.B. Douglas, N. Sherman, A. Seeber, N. Wright, Y. Güzükara, Towards effective phosphorus recycling from wastewater: quantity and quality, Chemosphere. 91 (2013) 676–684, https://doi.org/10.1016/j.chemosphere.2013.01.057.

[45] D. Crutchik, N. Morales, J.R. Vázquez-Padín, J.M. Garrido, Enhancement of struvite pellets crystallization in a full-scale plant using an industrial grade magnesium product, Water Sci. Technol. 75 (2017) 609–618, https://doi.org/10.2166/wst.2016.527.

[46] M.M. Seckler, M.L.J. Van Leeuwen, O.S.L. Bruinsma, G.M. Van Rosmalen, Phosphate removal in a fluidized bed - II process optimization, Water Res. 30 (1996) 1589–1596, https://doi.org/10.1016/0043-1354(96)00017-6.

[47] T. Zhang, R. Jiang, Y. Deng, Phosphorus recovery by struvite crystallization from livestock wastewater and reuse as fertilizer: a review, Physico-Chemical Wastewater Treat. Resour. Recover. InTech, 2017, pp. 135–152, https://doi.org/10.5772/65692.

[48] E. Tarragó, S. Puig, M. Ruscalleda, M.D. Balaguer, J. Colprim, Controlling struvite particles' size using the up-flow velocity, Chem. Eng. J. 302 (2016) 819–827, https://doi.org/10.1016/j.cej.2016.06.036.

[49] B. Tansel, G. Lunn, O. Monje, Struvite formation and decomposition characteristics for ammonia and phosphorus recovery: a review of magnesium-ammonia-phosphate interactions, Chemosphere 194 (2018) 504–514, https://doi.org/10.1016/j.chemosphere.2017.12.004.

[50] M.A. Lovette, M.F. Doherty, Needle-shaped crystals: causality and solvent selection guidance based on periodic bond chains, Cryst. Growth Des. 13 (2013) 3341–3352, https://doi.org/10.1021/cg301830u.

[51] M. Iqbal, H. Bhuiyan, D.S. Mavinic, Assessing struvite precipitation in a pilot-scale fluidized bed crystallizer, Environ. Technol. 29 (2008) 1157–1167, https://doi.org/10.1080/09593330802075452.

[52] J.P. Andreassen, M.J. Hounslow, Growth and aggregation of vaterite in seeded-batch experiments, AIChE J. 50 (2004) 2772–2782, https://doi.org/10.1002/aic.10205.

[53] C. Fang, T. Zhang, R. Jiang, H. Ohtake, Phosphate enhance recovery from wastewater by mechanism analysis and optimization of struvite settleability in fluidized bed reactor, Sci. Rep. 6 (2016) 32215, https://doi.org/10.1038/srep32215.

[54] S. Pilli, P. Bhunia, S. Yan, R.J. LeBlanc, R.D. Tyagi, R.Y. Surampalli, Ultrasonic pretreatment of sludge: a review, Ultrason. Sonochem. 18 (2011) 1–18, https://doi.org/10.1016/j.ultsonch.2010.02.014.

[55] L. Wei, T. Hong, H. Liu, T. Chen, The effect of sodium alginate on struvite crystallization in aqueous solution: a kinetics study, J. Cryst. Growth 473 (2017) 60–65, https://doi.org/10.1016/j.jcrysgro.2017.03.039.

[56] Z.L. Ye, Y. Deng, X. Ye, Y. Lou, S. Chen, Application of image processing on struvite recovery from swine wastewater by using the fluidized bed, Water Sci. Technol. 77 (2018) 159–166, https://doi.org/10.2166/wst.2017.533.

[57] A.P. Collier, M.J. Hounslow, Growth and aggregation rates for calcite and calcium oxalate monohydrate, AIChE J. 45 (1999) 2298–2305, https://doi.org/10.1002/aic.690451105.

[58] E. European, Sustainable Phosphorus Platform, ESPP 2016, (2016).

[59] Y. Liu, H. Qu, Interplay of digester supernatant composition and operating pH on impacting the struvite particulate properties, J. Environ. Chem. Eng. 5 (2017) 3949–3955, https://doi.org/10.1016/j.jece.2017.07.065.

[60] R.M. Smith, A.E. Martell, R.J. Motekaitis, NIST Critically Selected Stability Constants of Metal Complexes Database, (2004), https://doi.org/10.3938/jkps.51.112.